Generation and detection of a sub-Poissonian atom number distribution in a one-dimensional optical lattice

J.-B. Béguin, E. M. Bookjans, S. L. Christensen, H. L. Sørensen, J. H. Müller, J. Appel,* and E. S. Polzik*
QUANTOP, Niels Bohr Institute, University of Copenhagen, Blegdamsvej 17, 2100 Copenhagen, Denmark
(Dated: October 16, 2014)

We demonstrate preparation and detection of an atom number distribution in a one-dimensional atomic lattice with the variance −14 dB below the Poissonian noise level. A mesoscopic ensemble containing a few thousand atoms is trapped in the evanescent field of a nanofiber. The atom number is measured through dual-color homodyne interferometry with a pW-power shot noise limited probe. Strong coupling of the evanescent probe guided by the nanofiber allows for a real-time measurement with a precision of ±8 atoms on an ensemble of some 10^3 atoms in a one-dimensional trap. The method is very well suited for generating collective atomic entangled or spin-squeezed states via a quantum non-demolition measurement as well as for tomography of exotic atomic states in a one-dimensional lattice.

PACS numbers: 42.50.Ct, 37.10.Jk, 42.50.Ex
Keywords: Quantum Optics, Fano factor, Nanofiber, QND measurement

arXiv:1408.1266v2 [quant-ph] 15 Oct 2014

Atoms trapped in an optical lattice are a well-pursued platform for the realization of a quantum simulator and quantum information processing devices [1]. In addition, mesoscopic ensembles of periodically well-separated atoms strongly coupled to light are an excellent arrangement for quantum metrology and sensing applications using collective atomic state entanglement [2].

The recent spectacular progress with cold atoms trapped in the evanescent field emanating from a tapered optical nanofiber with a sub-wavelength diameter [3–6] offers a realistic and promising implementation of a one-dimensional (1D) optical lattice efficiently coupled to a single well-defined light mode. Together with the mature technology of interconnecting optical fibers, atomic ensembles trapped around nanofibers have the potential to play an integral part in the construction of complex quantum networks. Photons propagating in a fiber connect hybrid quantum systems by interacting with various realizations of quantum systems, such as solid state systems and atoms, through strong light-matter coupling at nano-tapered fiber nodes [7, 8].

An efficient quantum interface between light and collective degrees of freedom of an atomic ensemble requires a high optical depth and a measurement sensitivity limited by the shot noise of light and the projection noise of atoms [9]. Under these conditions a quantum non-demolition (QND) measurement of atomic population differences has been used for the generation of spin squeezed [10], entangled states to improve atomic clocks [11, 12] and magnetometers [13, 14]. In addition, optical probing of atoms in one-dimensional lattices with sub-Poissonan precision has been proposed as a valuable measurement tool for strongly correlated systems [15]. The preparation of ensembles with narrow atom number distribution in atom traps and the knowledge of its statistics in real-time is also a well-recognized goal for quantum gate implementations based on collective Rydberg excitations [16, 17] or atomic Bragg mirrors [18]. For these and other applications it is desirable to have a probing and preparation method at hand which not only is minimally-destructive but also widely tunable in bandwidth. Ideally, it should enable monitoring dynamics on different timescales and to outrun the influence of any decoherence not caused by the measurement itself. While impressive atom number resolution has been reported for atomic ensembles inhomogeneously coupled to an optical cavity mode [19] and for ensembles trapped inside a low-noise magneto-optical trap [20], we demonstrate a fast single-pass atom number measurement method that is readily adapted to different measurement and preparation tasks in 1D ensembles.

In this work, we realize the first real-time, minimally-destructive detection of atoms with sub-Poissonian sensitivity in a 1D nanofiber lattice trap. Due to the guiding of the probe light by the nanofiber, the optical depth $N_{\mathrm{at}}\sigma/A$ achieves maximal values for a given atom number N_{at} as the light beam cross section A becomes comparable to the atomic cross section. The minimally destructive measurement is achieved by balancing the phase information obtained from atoms against the measurement back action, combined with quantum noise limited sensitivity for both probe photons and atoms. Through a continuous shot noise limited measurement of the atom induced phase shift of light, we resolve and prepare an atom number distribution of the ensemble with a minimum Fano factor $(\Delta N_{\mathrm{at}})^2/N_{\mathrm{at}}$ of −14 dB. The reduction of the atom number noise compared to the Poisson distribution is ultimately limited only by probe induced stochastic loss of atoms [21–23]. The absolute number of atoms in the lattice trap is calibrated accurately via a robust experimental method based on optical pumping [24]. Finally, we show that the achieved light-atom coupling strength and quantum noise limited sensitivity is suitable for quantum state tomography and will al-

low for the generation of many-body entangled states by QND measurements in our system.

In the experiment Cesium atoms are prepared in a nanofiber trap. Two counter-propagating red-detuned fields with a wavelength of $\lambda_{\rm red} = 1057\,$nm and a total power of $P_{\rm red} = 2 \times 1\,$mW together with an orthogonally linearly polarized blue-detuned running-wave field (with $\lambda_{\rm blue} = 780\,$nm, $P_{\rm blue} = 10\,$mW) are sent through an optical nanofiber and form two one-dimensional optical lattices [4]. With a nominal nanofiber diameter of $d = 500\,$nm, the trapping sites are located 200 nm above the surface of the fiber. A magneto-optical trap (MOT) is superimposed on the fiber; atoms are loaded into the lattice trap after a sub-Doppler cooling phase, during which they are pumped into the hyperfine ground state $|3\rangle \equiv (6^2S_{1/2}, F = 3)$. Immediately before probing, the atoms are pumped back to the $|4\rangle \equiv (6^2S_{1/2}, F = 4)$ state with external repuming light tuned to the $|3\rangle \rightarrow |4'\rangle \equiv (6^2P_{3/2}, F = 4)$ transition.

Our atom number preparation and real-time measurement procedure relies on the detection of a differential phase shift imprinted by the atoms on two probe light fields propagating in the fundamental mode of the fiber. The two probes are detuned symmetrically around the atomic resonance by $\pm\Omega$, balanced in power and linearly polarized as the 1057 nm trap field. They are generated from an acousto-optic modulator (AOM) in the Raman-Nath regime before they are recombined in a common spatial mode, see Fig. 1a. Due to the anti-symmetric nature of the atomic dispersion (Fig. 1b), the probes have acquired phase shifts of opposite sign after interacting with the atoms at the fiber nanotaper. Measuring the differential phase shift between the two probes yields a signal proportional to the number of interacting atoms. At the same time, any common-mode optical path-length and polarization fluctuation noise is canceled. Furthermore, inhomogeneous differential Stark shifts imprinted on the atoms by off-resonant probing are suppressed [25].

After passage through the atomic ensemble, the differential phase shift between the two probes is measured using optical homodyne interferometry, see Fig. 1a; the two probes are overlapped with a strong optical local oscillator (LO) on a 90:10 beam splitter, and the signal is detected with a photo-detector peaked around the beat-note frequency Ω. Because of the symmetrical placement of the probe sidebands with respect to the LO the usual 3 dB noise penalty for heterodyne detection is avoided [26]. The detected beat-note in the photocurrent is mixed down to baseband electronically and both differential phase shift and common-mode attenuation of the probe light are extracted from the signal. All optical fields used for probing are derived from the same laser source and the optical phase of the LO is stabilized to the point of highest differential phase sensitivity by a slow servo loop.

Since in homodyne detection the signal strength and

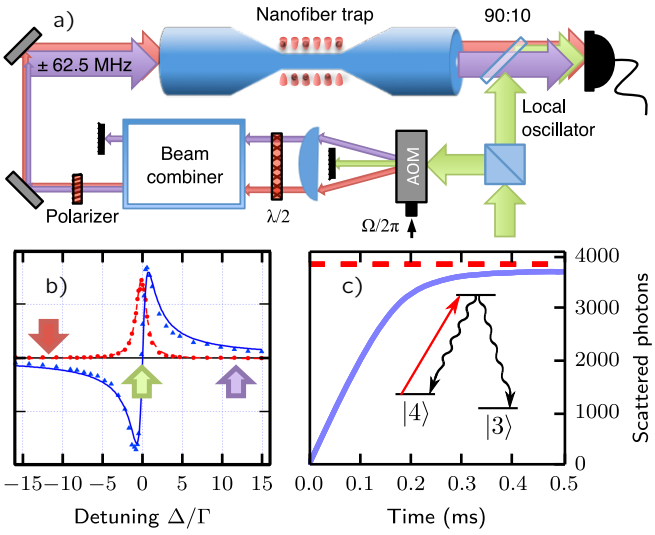

Figure 1. a) Experimental setup. Two 1D optical lattices are formed in the nanofiber trap by two trapping beams (not shown). Two probe beams with fixed frequency difference are generated with an AOM and then coupled into the nanofiber where they interact with the atomic ensemble. They interfere with a strong LO on a 90:10-beam splitter and a homodyne measurement is performed. b) Absorption (red dots) and dispersion signals (blue triangles) measured with trapped atoms; arrows indicate probe and LO frequencies. c) Atom number calibration. Resonant light pumps atoms from $|4\rangle$ to $|3\rangle$. The total number of trapped atoms is determined from the decay branching ratio (see inset) and the asymptote (red dashed line) of the cumulative number of scattered photons (solid blue line, average of 200 experiments).

the photon shot noise contribution from the LO scale identically, technical noise sources can be overcome in a high detection bandwidth by using a sufficiently high LO power. The ultimate signal-to-noise ratio (SNR) with coherent light states is therefore only limited by the intrinsic quantum noise of the probes. In our experiment, LO photon shot noise dominates residual electronic noise typically by a factor of 3.5. This, together with other imperfections, translates into a minimum phase uncertainty $\delta\varphi$ slightly above the standard quantum limit expressed as

$$\delta\varphi = \frac{1}{2\sqrt{qN_{\rm ph}}}, \quad q \equiv \epsilon(1-l)\mathcal{V}\eta. \tag{1}$$

Here $N_{\rm ph}$ is the total number of probe photons at the atoms during the measurement probe time and q is an overall quantum efficiency, dependent on the quantum efficiency of the detector ϵ, the losses of the probe from the atoms to the detector l, the mode overlap of the probes and LO at the detector $\mathcal{V}$ and the ratio η of the LO shot noise to total detection noise [27]. A value of $q = 0.40 \pm 0.04$ is achieved in the experimental setup. We have verified the modeled performance of the detec-

tion scheme by a measurement of the Allan-deviation of interferometer phase in the absence of fiber-trapped atoms (for details, see SM : Dual-color homodyne detection).

By simply blocking one of the probe sidebands, the measurement scheme turns into standard heterodyne detection, which is used for initial calibration purposes [28]. With the remaining sideband tuned around the $|4\rangle \rightarrow |5'\rangle \equiv (6^2P_{3/2}, F' = 5)$ transition, the line shape and position of the optical resonance for trapped atoms is observed (see Fig. 1b). An energy absorption measurement with a single probe tuned to the $|4\rangle \rightarrow |4'\rangle$ transition is used to calibrate the number of trapped atoms. In other nanofiber trap experiments, the number of atoms has been estimated from the absorbed power of a probe beam fully saturating the trapped atoms [4, 5]. We apply a similarly robust but faster method, which allows to measure the atom number in a single run with adequate resolution and good accuracy, by recording optical pumping transients [29]. Atoms excited to the $|4'\rangle$ level decay with a fixed branching ratio into the $|4\rangle$ and $|3\rangle$ ground levels which allows to determine the number of atoms from the number of absorbed probe photons. From an average over 178 consecutive experimental runs, as shown in Fig. 1c, we find for the average number of trapped atoms $N_{\rm at} = 1606 \pm 4^{\rm stat} \pm 160^{\rm sys}$. The systematic error for this measurement is dominated by the fractional uncertainty of the overall quantum efficiency q.

To achieve the highest atomic response for the dual-color dispersive measurement the probes address the atoms in the $|4\rangle$ state through the excited $|5'\rangle$ state. We detune the probes by $\Omega = \pm 2\pi \cdot 62.5\,\mathrm{MHz} \approx \pm 12\Gamma$ from the atomic transition, where $\Gamma = 2\pi \cdot 5.23\,\mathrm{MHz}$ is the natural line width. This choice renders the atomic sample sufficiently transparent to couple all atoms equally while keeping the influence of neighboring hyperfine levels small. From the measured phase shift for ensembles with calibrated atom number we infer an on-resonant optical depth of $\alpha_{\rm at} = 0.024$ for a single maximally polarized atom on the $|4\rangle \rightarrow |5'\rangle$ transition [30]. Comparing to earlier results obtained in a free space optical dipole trap with a related probing method [31], this represents an improvement of more than two orders of magnitude in the signal from a single atom.

To illustrate the wide tunability of strength and bandwidth of the measurement we show real-time measurements of the atomic phase shift probing on the $|4\rangle \rightarrow |5'\rangle$ transition with and without external repumping light for varying probe powers in Fig. 2. In the shown range the maximum observed atomic phase shift is independent of the probe power as expected from the calculated saturation power of 224 nW at the used probe detuning. The probe-induced signal decay can be made much faster than the unperturbed trap lifetime without compromising signal strength by saturating the atoms. The data presented in Fig. 2 are taken on a trap with $1/e$ lifetime

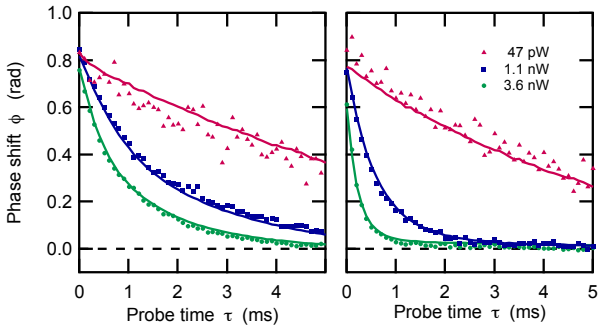

Figure 2. Real-time high SNR detection of atomic phase shift with weak coherent probe light for different powers. (symbols) Real-time phase shift data in a 100 kHz detection bandwidth; (solid lines) Average over 200 lattice trap preparations in the same detection bandwidth;(left panel) external repumping light on; (right panel) external repumping light off; Used probe powers are the same for both panels; probing starts 1 ms after trap loading.

in the absence of probing of $\tau_{\rm bg} = 6.8\,\mathrm{ms}$ [32]. Curiously, we observe that the probe induced loss rate grows slower than linear with the photon flux. The average numbers of scattering events $n_{\rm heat}$ to remove an atom from the trap are found to be $n_{\rm heat} \simeq 380$ for $P = 3.6\,\mathrm{nW}$, while $n_{\rm heat} \simeq 190$ for $P = 1.1\,\mathrm{nW}$ and $n_{\rm heat} \simeq 56$ only for $P = 0.15\,\mathrm{nW}$. Plain recoil heating in individual trap sites of calculated depth $10^3\ E_{\rm recoil}$ predicts constant $n_{\rm heat} \simeq 500$ [33] and clearly cannot explain the data. This peculiar behavior is not understood at present and is subject to further studies. In the absence of repumping light, probe-induced hyperfine pumping into the atomic state $|3\rangle$ is observed on average after $n_{\rm hf} = 67$ spontaneous emission events, in good agreement with the calculated value at the used probe detuning.

We now apply the calibrated dispersive minimally-destructive probing method to prepare atom number distributions in the optical lattice with sub-Poissonian fluctuations. The Fano factor quantifies the reduction in the atom number fluctuations as compared to a Poisson distribution as $F = (\Delta N_{\rm at})^2 / \langle N_{\rm at} \rangle$. A Fano factor below unity is sometimes referred to as number squeezing. In the experiment atoms are probed 10 ms after the sub-Doppler cooling to avoid transit signals from untrapped atoms from the initial MOT reservoir. Atoms are probed on the $|4\rangle \rightarrow |5'\rangle$ transition and external repumping light on the $|3\rangle \rightarrow |4'\rangle$ transition is used to counteract hyperfine pumping. In Fig. 3 we show a typical record of the measured real-time phase shift from a single realization where data points are averaged over 5 µs. The noisy data is seen to follow a smoothly decaying curve with time or equivalently the probe photon number. We apply a recursive Bayesian estimation procedure to track the atom number distribution at a given invested probe photon number $N_{\rm ph}$ from all phase measurement data up to that

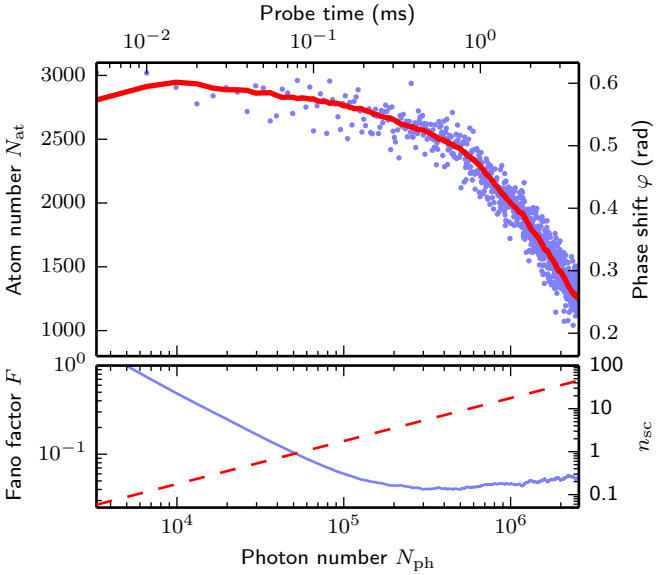

Figure 3. Top: Recursive Bayesian estimation of the atom number distribution. Blue dots: atom induced optical phase shift φ, as measured in a single experiment with the dual-color homodyne technique. Red line: mean of the estimated probability distribution for $N_{\rm at}$ at every time. Bottom: Solid blue line: Fano factor $F = \mathrm{var}(N_{\rm at})/\langle N_{\rm at}\rangle$ from the same probability distribution. Dashed red line: number of scattered photons $n_{\rm sc}$ per atom. All data were recorded with a probe power of 154 pW, 10 ms after the MOT cooling phase.

time (see SM : Recursive Bayesian estimation of the atom number): We describe our knowledge of the atom number by an initially uniform probability distribution. With every sample of acquired, shotnoise-contaminated data, we update this distribution using Bayes rule of inference. In every step, we evolve our estimator distribution to account for stochastic loss of atoms due to background gas collisions and due to heating by the probe light. The lower panel in Fig. 3 displays the Fano factor for the atom number estimator. We find a minimum Fano factor of -14 dB from the knowledge acquired by 5×10^5 probe photons which led to a loss of only 14 % of the initial atoms. This demonstrates that we can prepare ensembles with arbitrary atom numbers between $1000-2500$ with Fano factors well below -10 dB.

For the preparation of the total trapped atom number, a strong measurement can be applied, since the only back-action mechanism changing the variable of interest is atom loss due to recoil heating. Tomographic characterization of collective atomic hyperfine coherence by measuring atomic population differences instead does not allow for the use of repump light [34]. Preparation of spin-squeezed ensembles by a QND measurement is even more stringent and limits the number of allowed spontaneous emission events below unity [10, 12].

We use a simplified model for the variance of the atom number estimator, inspired by [19], in order to evaluate the potential of the measurement scheme for the different tasks. Assuming that all atom loss is caused by probe light, the variance of the estimator writes as

$$(\Delta N_{\rm at})^2 = \left(\frac{1}{(\Delta N_{\rm at}^{\rm i})^2} + q\alpha_{\rm at} n_{\rm sc}\right)^{-1} + N_{\rm at}\frac{n_{\rm sc}}{n_{\rm loss}}. \quad (2)$$

Here, $\alpha_{\rm at}$ denotes the single-atom optical depth on the probe transition, $n_{\rm sc}$ is the number of probe photons scattered into free space for a single atom, $(\Delta N_{\rm at}^{\rm i})^2$ is the initial variance of the atomic ensemble before probing, and $n_{\rm loss}$ the critical number of scattering events, i.e. $n_{\rm heat} = 56$ for atom number preparation as in Fig. 3, $(n_{\rm hf}^{-1} + n_{\rm heat}^{-1})^{-1}$ for state tomography and $n_{\rm loss} \lesssim 1$ for conditional spin-squeezing. Any initial information about the atom number distribution is encoded in the prior variance $(\Delta N_{\rm at}^{\rm i})^2$. The first term describes the gain of knowledge from the phase shift measurement while the second term reflects the noise from stochastic atom loss.

The measurement strength characterized by $n_{\rm sc}$, can now be optimized for all three tasks (see SM : Simplified model for atom number estimator variance). For atom number preparation we find $n_{\rm sc} = 2.4$ leading to a predicted minimum Fano factor of -11 dB for the parameters of Fig. 3. The simple model is somewhat pessimistic but still in reasonable agreement with the observed values.

In quantum state tomography where reduction of the variance has to be balanced with the noise introduced by heating and hyperfine pumping, the minimum predicted Fano factor is -8 dB. This should be compared with -3 dB required to observe negative Wigner function ensemble distributions and hence allows characterization of non-classical spin states for ensembles containing 2500 atoms. Extrapolating to measurement-based preparation of spin-squeezed collective atomic states, where we need to take the damping of hyperfine coherence due to photon scattering into account, we find that metrologically relevant squeezing up to -4.2 dB in our system is achievable if all other decoherence channels are negligible.

In conclusion, we have demonstrated an efficient interface between fiber-guided light modes and atomic ensembles trapped in a 1D optical lattice. The nanofiber trap geometry offers two obvious routes for future improvements. The single atom coupling strength can be moderately increased by pulling atoms closer to the fiber surface, but also substantially increased by embedding the trap into an optical resonator using integrated fiber Bragg gratings [7, 35]. Alternatively, the ensemble size can be increased by simply using longer fiber sections without compromising the single atom coupling. At least one order of magnitude larger ensembles are realistic with current state of the art nanofiber production technology.

We gratefully acknowledge Prof. A. Rauschenbeutel and his group for advice and access to their fiber pulling rig and thank Prof. M. F. Andersen for fruitful and enlightening discussions. This work has been supported by

the ERC grant INTERFACE, the US ARO grant No. W911NF-11-0235 and the EU grant SIQS.

[1] I. Bloch, J. Dalibard, and S. Nascimbène, Nature Physics **8**, 267 (2012).
[2] V. Giovannetti, S. Lloyd, and L. Maccone, Nature Photonics **5**, 222 (2011).
[3] F. Le Kien, V. I. Balykin, and K. Hakuta, Phys. Rev. A **70**, 063403 (2004).
[4] E. Vetsch, D. Reitz, G. Sagué, R. Schmidt, S. T. Dawkins, and A. Rauschenbeutel, Phys. Rev. Lett. **104**, 203603 (2010).
[5] A. Goban, K. S. Choi, D. J. Alton, D. Ding, C. Lacroûte, M. Pototschnig, T. Thiele, N. P. Stern, and H. J. Kimble, Phys. Rev. Lett. **109**, 033603 (2012).
[6] S. T. Dawkins, R. Mitsch, D. Reitz, E. Vetsch, and A. Rauschenbeutel, Phys. Rev. Lett. **107**, 243601 (2011).
[7] K. P. Nayak, P. Zhang, and K. Hakuta, Opt. Lett. **39**, 232 (2014).
[8] M. Hafezi, Z. Kim, S. L. Rolston, L. A. Orozco, B. L. Lev, and J. M. Taylor, Phys. Rev. A **85**, 020302 (2012).
[9] K. Hammerer, A. S. Sørensen, and E. S. Polzik, Rev. Mod. Phys. **82**, 1041 (2010).
[10] J. Appel, P. J. Windpassinger, D. Oblak, U. Busk Hoff, N. Kjærgaard, and E. S. Polzik, P. Natl. Acad. Sci. **106**, 10960 (2009).
[11] A. Louchet-Chauvet, J. Appel, J. J. Renema, D. Oblak, N. Kjaergaard, and E. S. Polzik, New. J. Phys. **12**, 065032 (2010).
[12] M. H. Schleier-Smith, I. D. Leroux, and V. Vuletić, Phys. Rev. Lett. **104**, 073604 (2010).
[13] W. Wasilewski, K. Jensen, H. Krauter, J. J. Renema, M. V. Balabas, and E. S. Polzik, Phys. Rev. Lett. **104**, 133601 (2010).
[14] M. Koschorreck, M. Napolitano, B. Dubost, and M. W. Mitchell, Phys. Rev. Lett. **104**, 093602 (2010).
[15] K. Eckert, O. Romero-Isart, M. Rodriguez, M. Lewenstein, E. S. Polzik, and A. Sanpera, Nature Physics **4**, 50 (2008).
[16] M. Saffman, T. G. Walker, and K. Mølmer, Rev. Mod. Phys. **82**, 2313 (2010).
[17] D. Petrosyan and G. M. Nikolopoulos, Phys. Rev. A **89**, 013419 (2014).
[18] D. E. Chang, L. Jiang, A. V. Gorshkov, and H. J. Kimble, New. J. Phys. **14**, 063003 (2012).
[19] H. Zhang, R. McConnell, S. Ćuk, Q. Lin, M. H. Schleier-Smith, I. D. Leroux, and V. Vuletić, Phys. Rev. Lett. **109**, 133603 (2012).
[20] D. B. Hume, I. Stroescu, M. Joos, W. Muessel, H. Strobel, and M. K. Oberthaler, Phys. Rev. Lett. **111**, 253001 (2013).
[21] A. Itah, H. Veksler, O. Lahav, A. Blumkin, C. Moreno, C. Gordon, and J. Steinhauer, Phys. Rev. Lett. **104**, 113001 (2010).
[22] Y. R. P. Sortais, A. Fuhrmanek, R. Bourgain, and A. Browaeys, Phys. Rev. A **85**, 035403 (2012).
[23] S. Whitlock, C. F. Ockeloen, and R. J. C. Spreeuw, Phys. Rev. Lett. **104**, 120402 (2010).
[24] W. Ketterle, K. B. Davis, M. A. Joffe, A. Martin, and D. E. Pritchard, Phys. Rev. Lett. **70**, 2253 (1993).
[25] M. Saffman, D. Oblak, J. Appel, and E. S. Polzik, Phys. Rev. A **79**, 023831 (2009).
[26] M. Locke and C. Fertig, JOSA B **30**, 2409 (2013).
[27] J. Appel, D. Hoffman, E. Figueroa, and A. I. Lvovsky, Phys. Rev. A **75**, 035802 (2007).
[28] J. M. Pino, R. J. Wild, P. Makotyn, D. S. Jin, and E. A. Cornell, Phys. Rev. A **83**, 033615 (2011).
[29] Y.-C. Chen, Y.-A. Liao, L. Hsu, and I. A. Yu, Phys. Rev. A **64**, 031401 (2001).
[30] We assume here that the dispersively probed ensemble is unpolarized.
[31] S. L. Christensen, J.-B. Béguin, E. Bookjans, H. L. Sørensen, J. H. Müller, J. Appel, and E. S. Polzik, Phys. Rev. A **89**, 033801 (2014).
[32] For the data presented in Fig. 3, intensity noise of the trap lasers has been reduced significantly which led to a longer trap lifetime of 20 ms.
[33] S. Wolf, S. J. Oliver, and D. S. Weiss, Phys. Rev. Lett. **85**, 4249 (2000).
[34] S. L. Christensen, J. B. Béguin, H. L. Sørensen, E. Bookjans, D. Oblak, J. H. Müller, J. Appel, and E. S. Polzik, New J. Phys., Focus issue on Quantum Tomography **15**, 015002 (2013).
[35] C. Wuttke, M. Becker, S. Brückner, M. Rothhardt, and A. Rauschenbeutel, Opt. Lett. **37**, 1949 (2012)

SUPPLEMENTAL MATERIAL

Dual-color homodyne detection

We consider an idealized balanced homodyne setup with a strong local oscillator field E_{LO} and a dual-color probe field E_{signal} impinging on a 50 : 50 beam splitter. Both sidebands experience an phase shift by φ with opposite sign:

$$E_{\mathrm{LO}} = E_{\mathrm{L}} e^{i\omega t} \tag{S1}$$

$$E_{\mathrm{signal}} = E_1 e^{i(\omega+\Omega)t+i\varphi} + E_2 e^{i(\omega-\Omega)t-i\varphi} \tag{S2}$$

From the fields at the two beam splitter output ports $E_{\pm} = (E_{\mathrm{LO}} \pm E_{\mathrm{signal}})/\sqrt{2}$ we obtain the intensities:

$$I_{\pm} = |E_{\pm}|^2 = \frac{1}{2}|E_{\mathrm{LO}}|^2 + \frac{1}{2}|E_{\mathrm{signal}}|^2 \pm \mathrm{Re}\,(E_{\mathrm{LO}}^* E_{\mathrm{signal}}) \tag{S3}$$

The homodyne detector signal is obtained by subtracting the photocurrents in both arms and therefore it is proportional to

$$\Delta I = I_+ - I_- = 2\,\mathrm{Re}\,(E_{\mathrm{LO}}^* E_{\mathrm{signal}}). \tag{S4}$$

Inserting (S2) we obtain

$$\Delta I = 2\,\mathrm{Re}\Big[\quad E_{\mathrm{L}}^*(E_1+E_2)\cos(\Omega t+\varphi) \\ +iE_{\mathrm{L}}^*(E_1-E_2)\sin(\Omega t+\varphi) \quad \Big]. \tag{S5}$$

We choose the local oscillator phase to be real $E_{\mathrm{L}} = \sqrt{I_{\mathrm{LO}}}$ and balance the sideband powers, so that $E_1 = E_2 = \sqrt{I_{\mathrm{s}}/2}$ and obtain a beat signal at frequency $\Omega/2\pi$ phase shifted by the optical sideband phase shifts φ:

$$\Delta I(t) = 2\sqrt{2 I_{\mathrm{s}} I_{\mathrm{LO}}}\cos(\Omega t+\varphi). \tag{S6}$$

For phase detection, we integrate this signal over a time $\tau = 2\pi m/\Omega$ corresponding to m oscillation periods while we demodulate with $\sin(\Omega t)$. Designating κ as the conversion factor from optical intensities to photo-electron-flux the number of detected and demodulated photo-electrons is:

$$\Delta n_\tau^{\sin} = \int_0^\tau \kappa \Delta I(t)\sin(\Omega t)\,\mathrm{d}t \tag{S7}$$

$$= \kappa 2\sqrt{2 I_{\mathrm{s}} I_{\mathrm{LO}}}\int_0^\tau \cos(\Omega t+\varphi)\sin(\Omega t)\,\mathrm{d}t \tag{S8}$$

$$= -\kappa\tau\sqrt{2 I_{\mathrm{s}} I_{\mathrm{LO}}}\sin\varphi. \tag{S9}$$

Shot noise in the photocurrent limits the obtainable phase resolution to

$$\delta\phi = \frac{\delta\Delta n_\tau^{\sin}}{\left|\frac{\mathrm{d}\Delta n_\tau^{\sin}}{\mathrm{d}\varphi}\right|}, \tag{S10}$$

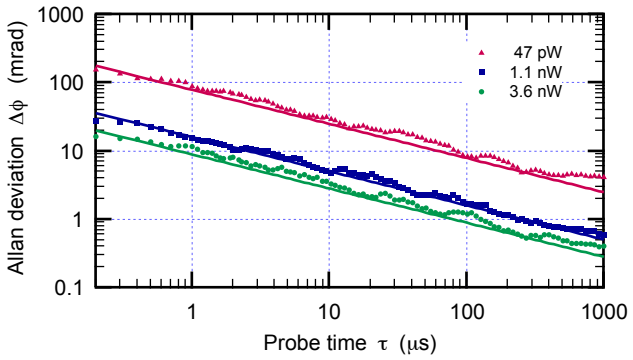

Figure S1. Log-log scale of the measured Allan deviation of the phase as a function of the probe time window τ for different probe powers at the location of the lattice trap. (Points) Experimental data (Solid lines) Expected theoretical quantum noise for the the overall quantum efficiency of detection $q = 0.40$ and probe power.

where $\delta\Delta n_\tau^{\sin}$ denotes shot noise fluctuations of $\Delta n_\tau^{\sin}$. The fluctuations of the cos- and sin demodulated components are equal in power and independent, and the powers add up to that of the vacuum fluctuations: $(\delta\Delta n_\tau^{\sin})^2 + (\delta\Delta n_\tau^{\cos})^2 = (\delta\Delta n_\tau)^2$. Since $I_{\mathrm{s}} \ll I_{\mathrm{LO}}$, in the balanced detection $\delta\Delta n_\tau = \delta n_\tau = \sqrt{n_\tau}$ where $n_\tau = \kappa\tau I_{\mathrm{LO}}$ is the total number of detected photons during the time τ. We therefore have

$$\delta\Delta n_\tau^{\sin} = \delta\Delta n_\tau^{\cos} = \frac{1}{\sqrt{2}}\sqrt{n_\tau} = \sqrt{\kappa\tau I_{\mathrm{LO}}/2}. \tag{S11}$$

From equations (S10) and (S11) we now obtain for the shot noise limited phase resolution in the dual-color homodyne setting:

$$\delta\varphi = \frac{\sqrt{\kappa\tau I_{\mathrm{LO}}/2}}{\kappa\tau\sqrt{2 I_{\mathrm{s}} I_{\mathrm{LO}}}} = \frac{1}{2\sqrt{\kappa\tau I_{\mathrm{s}}}} = \frac{1}{2\sqrt{n_{\mathrm{s}}}}. \tag{S12}$$

Here $n_{\mathrm{s}} = \kappa\tau I_{\mathrm{s}}$ is the total number of detected signal photons. We note that this result is identical with the limiting resolution in homodyne detection of the phase of a single-frequency coherent state with a mean photon number of n_{s}. In the main text we express the phase resolution in terms of the photon number sent through the atomic ensemble leading to eq. (1). To test the predicted minimal light shot noise limited phase resolution $\delta\varphi$, we measure the Allan phase deviation, $\Delta\phi$, in absence of atoms for different probe light powers (see Fig. S1). We find excellent agreement between measured and expected Allan deviation with the independently measured detection efficiency q.

Recursive Bayesian estimation of the atom number

The method of recursive Bayesian [36] estimation provides a framework to estimate a probability distribution

for the number of atoms during the process of probing based on the cumulative knowledge obtained by weak measurements. It is based on dividing the probing into discrete time intervals; in each interval the optical phase induced by the atoms is sampled. At the same time, the atom number in the probed level changes due to processes such as collisions with the background gas, probe-induced heating, optical pumping, etc.

In each time step l of duration Δt, we probe the ensemble with ΔN probe photons; the atom number evolution is modeled as a Markov process, so that each atom has a fixed probability P to "disappear", i.e. the probability to have N_l atoms in the trap in the i-th step given that the atom number was N_{l-1} in the previous step is governed by a binomial distribution:

$$p(N_l|N_{l-1}) = \binom{N_{l-1}}{N_l}(1-P)^{N_l}P^{N_{i-l}-N_l}, \tag{S13}$$

so that on average the atom number evolves as

$$\langle N_l\rangle = N_0 e^{-lP} = N_0 e^{-\frac{t}{\Delta t}P}. \tag{S14}$$

Also in each step, we obtain a new measurement of the optical phase shift φ proportional to the current atom number N_l with an added random Gaussian shot noise contribution ε with $\mathrm{var}\,\varepsilon = (\delta\varphi)^2$:

$$\varphi_l = kN_l + \varepsilon, \tag{S15}$$

so that φ_l is normally distributed:

$$p(\varphi_l|N_l) = \frac{1}{\sqrt{2\pi\,\mathrm{var}\,\varepsilon}} e^{-\frac{1}{2}\frac{(\varphi_l - kN_l)^2}{\mathrm{var}\,\varepsilon}}. \tag{S16}$$

Starting with an initial estimation of the atom probability $p(N_0)$, in each step we use the result of the new phase measurement φ_l to update our estimation:

$$p(N_i|\varphi_{1\ldots l}) = \alpha\, p(\varphi_l|N_l)\, p(N_l|\varphi_{1\ldots l-1}), \tag{S17}$$

where α normalizes $\sum_{N=0}^{\infty} p(N|\varphi_{1\ldots l}) = 1$ and

$$p(N_l|\varphi_{1\ldots l-1}) = \sum_{N_{l-1}=0}^{\infty} p(N_l|N_{l-1})p(N_{l-1}|\varphi_{1\ldots l-1}). \tag{S18}$$

For Fig. 3, we assume a uniform probability $p(N_0)$ for $N_i < 4400$ and calibrate P from fitting eq. (S14) to the mean atom number decay recorded in 200 separate experiments. In Fig. S2 we present the statistics of the achieved Fano factors obtained by Bayesian estimation of the atom number in those 200 experiments.

Atom number calibration method

To accurately determine the number of trapped atoms a single sideband resonant with the $|4\rangle \to |4'\rangle$ transition is used. In brief, the idea behind the measurement is as follows. An excited atom in any of the $|4'\rangle$ states can decay either to the $|3\rangle$ and $|4\rangle$ manifold. The branching ratio for this decay is independent of the Zeeman $m_{F'}$ sublevel. Because of the large ground state hyperfine splitting Cs atoms in the $|3\rangle$ state are far-detuned from the probe laser frequency and therefore do interact with the probe light only very weakly, i.e., atoms in this state do *not* absorb any photons from the probe to an excellent approximation. The number of trapped atoms in $|4\rangle$ will decrease with time during probing and the probe transmission will increase accordingly. To find

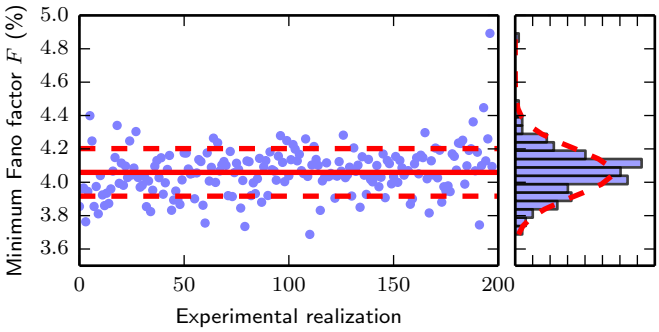

Figure S2. Left: minimum Fano factor F obtained in 200 successive experiments. Right: histogram.

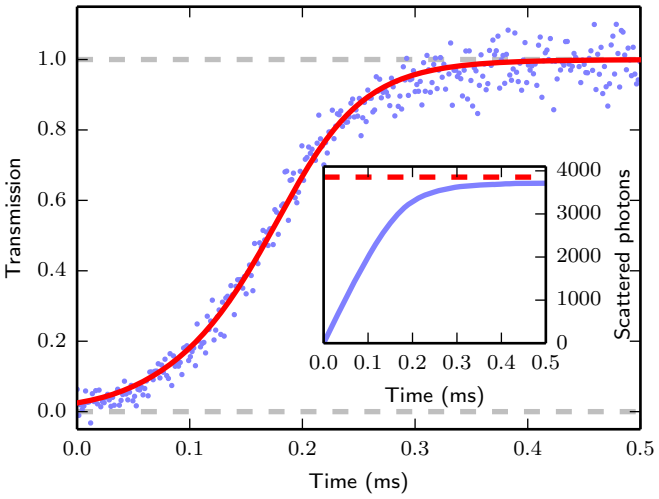

Figure S3. Calibration measurement of the absolute atom number in the lattice trap. An atom number of $N_{\mathrm{at}} = 1606 \pm 4^{\mathrm{stat}} \pm 160^{\mathrm{sys}}$ atoms is determined through optical pumping into a dark state via the integration of the total number of probe photons required to bleach the ensemble. The probe light is resonant with the atomic $|4\rangle \to |4'\rangle$ transition and the fiber-guided probe power at the atoms is 5.0 pW. The transmission is deduced from an heterodyne measurement of the two quadratures of the probe field. Signals are recorded 10 ms after the sub-Doppler cooling phase. The shown data is an average over 178 runs. The model fit estimates an associated on-resonance optical depth per atom of 1.64 % on the closed transition ($|4, m_F = 4\rangle \to |5', m_F = 5\rangle$).

the number of atoms we need to determine the number of scattering events it takes for the probe to reach full transmission. To model this, we consider a simple three level scheme and derive a differential equation for the optical depth, d, as this will directly give the transmission using the Lambert-Beer law. The number of atoms in the $|4\rangle$ state N_4 changes due to scattering events. We have with $\Phi_{\mathrm{in}}(\Phi_{\mathrm{out}})$ as the input (output) photon flux respectively,

$$\frac{\mathrm{d}N_4}{\mathrm{d}t} = -\frac{1}{k}\Big(\Phi_{\mathrm{in}}(t) - \Phi_{\mathrm{out}}(t)\Big). \tag{S19}$$

On average, it takes $k = 2.4$ scattering events to pump an atom from $|4\rangle$ to $|3\rangle$ as can be easily derived from the partial decay rates ($7/12\Gamma$, $5/12\Gamma$) of the $|4'\rangle$ states. The output photon flux follows Lambert-Beer's law

$$\Phi_{\mathrm{out}}(t) = \Phi_{\mathrm{in}}(t)\exp(-d(t)), \tag{S20}$$

where

$$d(t) \equiv N_{\mathrm{at}}(t)\alpha_{\mathrm{at}} \tag{S21}$$

is the optical depth, and α_{at} denotes the per-atom optical depth on the used transition. Combining eqs. (S19) to (S21), we obtain the desired differential equation for $d(t)$:

$$\frac{\mathrm{d}}{\mathrm{d}t}d(t) = -\frac{\alpha_{\mathrm{at}}}{k}\Phi_{\mathrm{in}}(t)\left[1 - \exp(-d(t))\right], \tag{S22}$$

Assuming a constant input flux, the solution is

$$d(t) = \ln\left[1 + \left(\mathrm{e}^{d(t=0)} - 1\right)\exp\left(-\alpha_{\mathrm{at}}\Phi_{\mathrm{in}}t/k\right)\right], \tag{S23}$$

from which we find for the sample transmission $T(t) = \mathrm{e}^{-d(t)}$ the expression for the fit model in Fig. S3.

$$T(N_{\mathrm{at}}, \alpha_{\mathrm{at}}, t) = \frac{1}{1 + \left[\exp\left(\alpha_{\mathrm{at}}N_{\mathrm{at}}\right) - 1\right]\exp\left(-\alpha_{\mathrm{at}}\Phi_{\mathrm{in}}t/k\right)}; \tag{S24}$$

allowing us to deduce both N_{at} and α_{at}.

Since the method is used to calibrate the atom number, possible systematic effects need to be addressed. Probe laser detuning, polarization, population redistribution among Zeeman sub-levels and inhomogeneous broadening of the probe transition by trap light do not influence the number of spontaneous emission cycles needed to bleach the sample and hence do not change the estimated atom number. The possible dark state in the Zeeman manifold of the $|4\rangle$ level, where population could be trapped, is avoided by a suitably oriented magnetic field. Modifications to the excited state decay rate caused by the close proximity to the dielectric surface of the fiber are small (below the percent level) and not expected to change the branching ratio to first order. Other systematic effects like radiation trapping, which has compromised the accuracy of the method in previous implementations with cold atoms, as well as collective backscattering are largely suppressed by the extreme 1D geometry and the incommensurate lattice and probe wavelengths. In practice, the largest systematic error by far stems from the calibration uncertainty of the overall quantum efficiency q and hence the input photon flux to the atomic sample, which amounts to 10% in our experiment. We note that this calibration error is not subject to fluctuations between consecutive experimental runs.

Several of the above mentioned parameters and effects systematically lower the *speed* of the optical pumping transient and hence bias the value for the fitted single atom coupling strength α_{at}. Similarly, atom number variations from run to run conspire to soften the sharp transition from almost complete absorption to full transmission when raw signals are averaged over many realizations. We observe a significant difference between coupling strength extracted from a fit to an averaged trace, as shown in Fig. S3, and the average coupling strength from fits to individual traces. The atom number estimate, instead, is robust against interchange of fitting and averaging operations. Comparing the average of inferred coupling strength values from individual fits to the coupling strength from dispersive phase shift measurements we find a remaining relative deviation of 25%.

Simplified model for atom number estimator variance

To arrive at the formula for the variance of the atom number estimator in eq. (2) we start by relating the phase resolution of the homodyne method eq. (1) to the atom number resolution given a number of photons scattered into free space n_{sc}. Coherent probe light passing through an ensemble of 2-level atoms with on-resonance optical depth $d_0 = \alpha_{\mathrm{at}} \cdot N_{\mathrm{at}}$ acquires a phase shift φ

$$\varphi = \frac{d_0}{2}\frac{\tilde{\Delta}}{1 + \tilde{\Delta}^2} \simeq \frac{d_0}{2}\tilde{\Delta}^{-1}, \tag{S25}$$

with $\tilde{\Delta}$ the detuning in units of half the natural linewidth $\Gamma/2$ and the approximation valid for the experimentally relevant case of $\tilde{\Delta} \gg 1$. In the same situation the probe photon flux $\dot{N}_{\mathrm{ph}}$ (equivalently photon number N_{ph} in a stationary situation) is reduced as

$$\frac{\Delta N_{\mathrm{ph}}}{N_{\mathrm{ph}}} = d_0\frac{1}{1 + \tilde{\Delta}^2} \simeq d_0\tilde{\Delta}^{-2}. \tag{S26}$$

Combining the two equations we get for an "ensemble" containing a single atom:

$$\varphi_1^2 = \frac{\alpha_{\mathrm{at}}}{4}\frac{n_{\mathrm{sc}}}{N_{\mathrm{ph}}}, \tag{S27}$$

where φ_1 denotes the phase shift due to a single atom.

The variance of the estimator for differential phase shift in a measurement using the dual-color homodyne method follows from eq. (1). Together with the phase shift of an ensemble containing N_{at} atoms $\varphi = N_{\mathrm{at}} \cdot \varphi_1$

this translates into the variance of the atom number estimator as

$$(\Delta\varphi)^2 = \frac{1}{4qN_{\rm ph}} \quad \Rightarrow (\Delta N_{\rm at})^2 = \frac{1}{4qN_{\rm ph}\varphi_1^2} \tag{S28}$$

and upon using eq. (S27)

$$(\Delta N_{\rm at})^2 = \frac{1}{q\alpha_{\rm at}n_{\rm sc}}. \tag{S29}$$

As expected for a dispersive measurement the variance does *not* depend on the atom number. Low variance is achieved with high quantum efficiency q, high single atom coupling strength $\alpha_{\rm at}$ and a high average scattered photon number. The estimator variance is seen to diverge when no measurement is performed, i.e. when $n_{\rm sc} \to 0$. From a Bayesian estimation perspective this corresponds to an uninformative prior. When doing a measurement, the variable of interest ($N_{\rm at}$) can change due to the back-action of the meter (probe light and vacuum modes) on the system (atomic ensemble). We incorporate Poissonian atom loss due to probe light scattering into free space and prior information about the atom number distribution, leading to

$$(\Delta N_{\rm at})^2 = \left(\frac{1}{(\Delta N_{\rm at}^{\rm i})^2} + q\alpha_{\rm at}n_{\rm sc}\right)^{-1} + N_{\rm at}\frac{n_{\rm sc}}{n_{\rm loss}}. \tag{S30}$$

as stated in eq. (2) of the main text.

A useful measurement reduces the variance of the estimator substantially with respect to the prior variance. Discarding the prior information for now, we optimize the measurement strength for a single step estimation of the atom number. Note that a single step estimation procedure performs worse than than the quasi-continuous Bayesian filtering method presented above, since the full variance of atom loss contributes despite the continuous monitoring. This explains the pessimistic predictions of the simplified estimator variance model. Working out the appropriate derivative, the minimum variance is achieved for a number $n_{\rm sc}$ of

$$n_{\rm sc} = \left(\frac{n_{\rm loss}}{N_{\rm at}q\alpha_{\rm at}}\right)^{1/2}, \tag{S31}$$

leading to minimum variance and minimum Fano factor as

$$(\Delta N_{\rm at})^2_{\rm min} = \left(\frac{4N_{\rm at}}{n_{\rm loss}q\alpha_{\rm at}}\right)^{1/2} \tag{S32}$$

$$F_{\rm min} = \left(\frac{4}{N_{\rm at}n_{\rm loss}q\alpha_{\rm at}}\right)^{1/2}. \tag{S33}$$

The numbers cited in the main text for atom number preparation (tomography) are calculated using $N_{\rm at} = 2500$ ($N_{\rm at} = 1250$) and $n_{\rm loss} = 56$ ($n_{\rm loss} = 30$) in eq. (S33). We assume here that tomographic characterization of the collective hyperfine coherence is performed with only 50% of the population residing in the coupled level.

For the extrapolation to measurement induced spin-squeezing the allowed measurement strength is so weak that the prior information becomes significant. In addition, for metrologically relevant squeezing the loss of hyperfine coherence (reduced Ramsey fringe contrast) needs to be taken into account properly, while the loss of atoms during the measurement is negligible for the weak measurement. We assume a coherent spin state of an ensemble with $N_{\rm at}$ 2-level atoms in the equatorial plane of the collective Bloch sphere as the initial condition. A weak measurement of the population of the upper level $|4\rangle$ is performed. Given this, the prior variance of the upper level population is $(\Delta N_{\rm at}^{\rm i})^2 = N_{\rm at}/4$. Scattering of probe photons reduces the contrast of fringes in a Ramsey experiment and hence the discriminator slope for a parameter measurement by a factor $\exp(-n_{\rm sc}/2)$, since only half of the atoms are probed. We take eq. (S30), neglect the atom loss term, normalize with the variance of the prior and correct for the loss of fringe contrast to get for the achievable squeezing ξ

$$\xi \equiv \frac{(\Delta N_{\rm at})^2}{N_{\rm at}/4}{\rm e}^{n_{\rm sc}} = \frac{1}{1 + q\alpha_{\rm at}N_{\rm at}n_{\rm sc}/4}{\rm e}^{n_{\rm sc}} \tag{S34}$$

or, in terms of the optical depth of the ensemble

$$\xi = \frac{1}{1 + qd_0n_{\rm sc}/4}{\rm e}^{n_{\rm sc}}. \tag{S35}$$

In the limit of high optical depth d_0 the squeezing is optimized for $n_{\rm sc} = 1$, equivalent to a reduction of Ramsey fringe contrast to 60%. To achieve any useful squeezing at all the product of optical depth and quantum efficiency needs to satisfy $qd_0 > 4$. For the numerical example of squeezing performance given in the main text, we use an ensemble size of $N_{\rm at} = 2500$ and assume atoms probed on the cycling transition leading to $\xi = -4.2\,$dB. This scenario is relevant for magnetic field sensing using the $|4,4\rangle$ to $|3,3\rangle$ hyperfine coherence.

[36] S. Särkkä, *Bayesian Filtering and Smoothing* (Cambridge University Press, 2013)